

Novel Tetrahedral Human Phantoms for Space Radiation Dose Assessment

Megan E. Chesal,¹ Rebecca S. Blue,^{2,3} Serena M. Aunon-Chancellor,^{3,4,5} and Jeffery C. Chancellor^{1,3,6,7}

¹*Department of Physics & Astronomy, Louisiana State University, Baton Rouge, LA, USA*

²*Aerospace Medicine and Vestibular Research Laboratory, The Mayo Clinic, Arizona; Scottsdale, AZ, USA;*

³*Department of Preventive Medicine & Population Health, University of Texas Medical Branch, Galveston, TX, USA*

⁴*Department of Internal Medicine, Louisiana State University Health Science Center, Baton Rouge, LA, USA*

⁵*Astronaut Office, NASA Johnson Space Center, Houston, TX, USA*

⁶*Outer Space Institute, University of British Columbia, Vancouver, CA*

⁷*Atlantis Industries, INC, USA**

Space radiation remains one of the primary hazards to spaceflight crews. The unique nature of the intravehicular radiation spectrum makes prediction of biological outcomes difficult, with computational simulation-based efforts stymied by lack of computational resources or accurate modeling capabilities. Recent advancements in both Monte Carlo simulations and computational human phantom developments have allowed for complex radiation simulations and dosimetric calculations to be performed for numerous applications. In this work, advanced tetrahedral-type human phantoms were exposed to a simulated spectrum of particles equivalent to a single days exposure in the International Space Station in Low Earth Orbit. 3D Monte Carlo techniques were used to produce and simulate the radiation spectra. Organ absorbed dose, average energy deposition, and the whole-body integral dose was determined for a male and female phantom. Results were then extrapolated for two long-term scenarios: a 6-9 month mission on the International Space Station and a 3-year mission to Mars. The whole-body integral dose for the male and female models were found to be 0.2985 ± 0.0002 mGy/day and 0.3050 ± 0.0002 mGy/day, respectively, which is within 10% of recorded dose values from the International Space Station. This work presents a novel approach to assess absorbed dose from space-like radiation fields using high-fidelity computational phantoms, highlighting the utility of complex models for space radiation research.

Introduction

The potential risks to human health incurred from prolonged exposure to the space radiation environment remains a primary limiting factor for long-duration space missions [1, 2]. The space radiation environment is a complex combination of fast-moving ions derived from all atomic species found in the periodic table [2]. These ionized nuclei have sufficient energy to penetrate a space-craft structure and cause deleterious biological damage to astronaut crews and other biological material, such as cell and tissue cultures [2, 3]. To date, our understanding of the nature of this risk, and impact to human health, remains incomplete. Further, there continues to be disparity between radiobiological studies and actual health outcomes seen in astronaut crews [2, 4].

Current space radiobiology studies primarily rely on animal model surrogates, translating interspecies results in an attempt to predict clinical outcomes for human physiology [4]. These animal studies have contributed to our understanding of disease mechanisms; however, their relevance to extrapolating outcomes in humans remains uncertain [2, 5–8]. It is believed that sufficient exposure to the complex space radiation environment could cause multi-organ dose toxicity, inhibiting cell regrowth and tissue repair mechanisms. Recent studies have demonstrated that the biological response and disease pathogenesis seen

after exposure to space radiation is unique to a nonhomogeneous, multi-energetic dose distribution [2, 3]. Thus, high-fidelity simulation of the complexity of the space environment and the human body is critical for accuracy in radiobiological experimental outcomes and terrestrial research. Current and historical calculations of space radiation biological impact have relied on more simplistic representations of human anatomy, the environment, and space radiation penetration and deposition in the body or individual organ systems due to previous limitations of calculations, phantom fidelity, or prediction of intravehicular spectra and dosage [9–12]. This has limited the success of dose prediction or in correlation to clinical outcome.

In this work, we present an approach involving computational human phantoms and their use in high-resolution and accurate dosimetry calculations for simulated exposure to the intravehicular space radiation environment similar to that incurred by astronauts onboard the International Space Station (ISS). Our goal is to numerically predict the dose in major organ and tissue volumes after a whole-body exposure to the space radiation environment. Use of high-fidelity human phantoms for more accurate computational reproduction of human space radiation exposures may help elucidate how the relative distribution of energy deposition and subsequent stress on organ systems such as the brain, lungs, and vasculature, may contribute to overall dose toxicity and potential health outcomes related to space radiation exposure.

*Electronic address: jchancellor1@lsu.edu

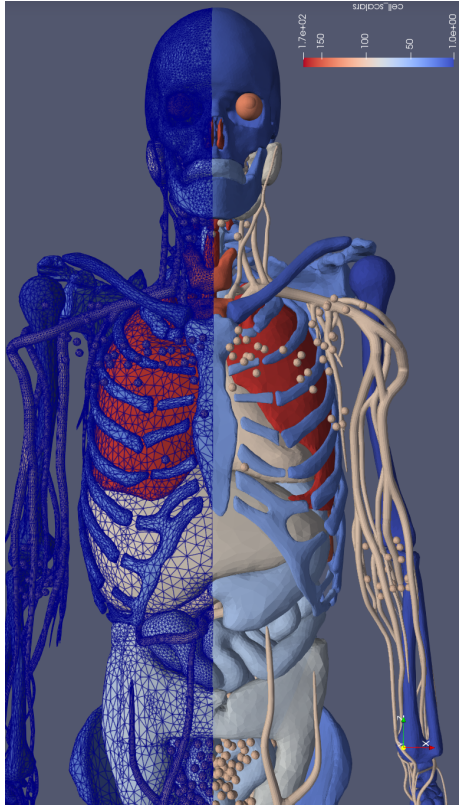


Figure 1: 90th Percentile Female Tetrahedral-Type Phantom. Tetrahedral-type phantoms are a progression of surface-type phantoms, with surface meshes replaced by volume tetrahedrons. Tetrahedral-type geometry is easily incorporated in Monte Carlo codes and leads to faster radiation transport calculations while still preserving the original complexity of surface phantoms. Shown here is the female tetrahedral-type phantom used in our calculations. In this view, the skin, muscles, and residual tissues are hidden to showcase internal anatomy structures. The right side of the phantom is visualized with smooth surfaces, while the left side is visualized as a surface with edges, showing the tetrahedrons that comprise the different model regions.

Background

The space radiation environment is comprised of a complex mixture of energetic radiation particulates that originate from both the sun and from outside of our solar system. Radiation emitted from the sun is comprised of electromagnetic, ultraviolet (UV), and X-ray radiation as well as the solar wind, which consists of protons and alpha particles and a small percentage of heavy-charged particles ($Z > 2$). Galactic Cosmic Rays (GCR) originate from outside of our solar system and are believed to be the remnants of supernova events [13]. Additionally, the low Earth orbit (LEO) radiation environment includes the Van Allen belts, toroidal regions comprised of electrons and protons. Vehicles (and crew) passing through these belts will incur additional exposure.

In nominal conditions within a shielded vehicle, the

primary source of radiation of concern to astronauts during long-duration deep space spaceflight is GCR [2]. The GCR spectrum is comprised mainly of protons and helium ions, though a smaller component, approximately one percent, consists of heavier and highly energetic nuclei with charges equal to or greater than atomic number $Z = 3$. While any ion species can be found in the GCR spectrum, the most prevalent ion species encountered are at or below $Z = 28$ [2, 13]. Although the contribution of these heavier ions to the total spectrum relative to protons and helium ions may be some orders of magnitude smaller, their potential biological impact is of equal or greater value [14, 15]. Energies of particles in the GCR spectrum can vary from kilo-electronvolts (keV) to several giga-electronvolts (GeV), energies sufficient to enable GCR particles to penetrate spacecraft shielding and interact with crewmembers [2, 12]. As GCR nuclei travel through spacecraft shielding, interactions will occur with the shielding medium. Such interactions can instigate energy loss mechanisms; in some cases, heavy ions may fragment into lighter ions with greater potential for biological damage or destruction than the original heavy ion. This creates a unique intravehicular (IVA) spectrum inside the spacecraft. The IVA spectrum can also include trapped charged particles due to the magnetic field surrounding the Earth; the relative contribution of these particles depends on the orbital flight path and how long a given vehicle remains in a region of trapped particles. For example, in certain trajectories the Van Allen belts can contribute significantly to total absorbed dose. While more shielding could be added to a vehicle to reduce the fluence of particles, payload lift capabilities limit the amount of material available. Additionally, studies have shown that dramatically increasing the shielding provides only limited reduction in particle fluence and could, in fact, increase the IVA radiation environment complexity [3].

The biological impact of radiation depends on a variety of physical and biological factors, including absorbed dose, dose rate, exposure time, particles species, material, and genetic variability. Computational simulations provide the capability for dosimetric calculations to be performed for simple and complex radiation spectra, either as a supplement to or in place of a physical experiment. Dose deposition in biological models can be simulated; however, to fully represent the complexity of such systems, high resolution models, or phantoms, should be utilized. Advancements in computational phantoms have allowed for the development of more complex models, allowing higher fidelity recreation of fine structures. The current premier phantoms are surface-type phantoms, where delineated organs and regions are defined by surface meshes [16–18]. In 2020, the International Commission on Radiological Protection (ICRP) published Report 145 which introduced two phantoms, an adult male and female polygonal surface mesh-reference computational phantom (MRCP), for use in dosimetric calculations [19]. Utilizing the ICRP MRCP models, Lee et. al. developed tetrahedral-type

phantoms representing the 90th percentile height and weight for male and female individuals for the worldwide Caucasian population [20].

Tetrahedral-type phantoms are advantageous for radiation transport simulations; they can be developed from medical images and detailed physical structures, such as lymph nodes, can be incorporated into the final phantom (as shown in Figure I). Deformation techniques, used to adjust select body regions for greater fidelity or to change a phantom positioning, can additionally be applied [21, 22]. Tetrahedral phantoms are created by applying mathematical techniques, such as Delaunay triangulation, to a surface-mesh that convert phantom structures to volumes defined by a series of tetrahedrons [23]. Figure II demonstrates how complex and minuscule surfaces can be defined with smooth edges; boundaries for organs are well defined in this manner. Further, these high-fidelity models are amenable to the incorporation of three-dimensional Monte Carlo particle transport software.

Here we utilize the tetrahedral-type phantoms developed by Lee et. al. and incorporate the Particle and Heavy Ion Transport Code System (PHITS), a three-dimensional radiation transport Monte Carlo platform with an event generator mode capable of simulating particles up to 200 GeV/n [24–26]. Incorporation of PHITS software into the advanced phantoms can allow for high-fidelity computation of dose deposition during spaceflight.

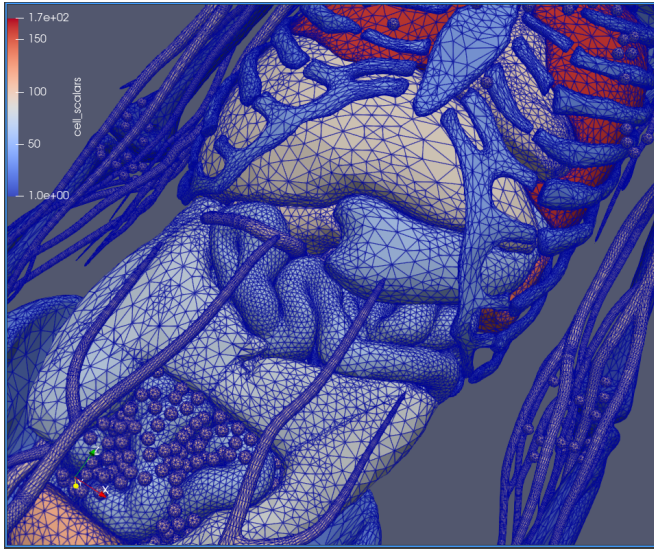


Figure II: Tetrahedral-Type Phantom Midsection Detail Tetrahedral-type phantoms are constructed with volumes filled with varying sized tetrahedrons. In the image, the lines on the organs represent the various tetrahedrons used to define that volume. Volumes and regions defined in this manner depend only on the size of the tetrahedrons, which is unlimited by modeling technique. While in large organs finely detailed tetrahedrons may not be needed, small or complex structures, such as mucosal linings, benefit greatly from a smaller-volume tetrahedron approach and can be modeled at the micrometer level.

Methods

Male and female 90th percentile mass and height surface phantoms were tetrahedralized by defined regions. Each phantom was individually exposed to a simulated IVA space radiation spectrum. To recreate the IVA spectrum, each individual simulated particle was transported through the phantom as an independent event, with energy reflecting IVA linear energy transport (LET) and particle spectrum as measured onboard the ISS Columbus Module in a "moderator block" technique previously described by Chancellor et. al. [12]. The spectrum generation method proposed by Chancellor et. al. uses charged particle interactions, specifically energy loss and spallation, to change the output of a heavy ion beamline to a more complex spectra. In the design proposed, 1 GeV iron ions pass through a moderation material of variable thickness, fragmenting the ions and reducing the energy of the primary ions and the produced ions such that the LET spectra and charged particle distribution produced matches measurements taken on ISS. The results were compared to measurements taken onboard ISS and found to be within excellent agreement [12, 27]. The moderation device was modeled in the 3D Monte Carlo software PHITS and the resulting spectra was recorded a meter behind the end of the block. The particle positions and directions were then reassigned to create a homogeneous exposure representative of the average environment on ISS.

All simulations were performed via PHITS and utilized high performance computers with parallel computational capacity. The average absorbed dose in each defined region was determined and additional tallies were set to record the three-dimensional dose distribution at two resolutions, 0.8 mm³ and 0.2 cm³.

Absorbed dose and average energy deposition was determined for all organ sites. Absorbed dose was calculated with the standard definition of energy deposition per unit mass for defined volume, and the whole body dose was calculated using the integral dose, in which the total energy deposited over the phantom was divided by the total mass of the phantoms [28]. Due to software limitations at the time of computation, the material surrounding the phantoms was approximated by low density air, with a density of 10^{-6} g/cm³, to minimize energy loss of the particles before interaction with the phantoms.

Figure III represents the 0.2 cm³ measured dose distribution, where dose external to the phantom is disregarded. Average regional doses were exported with relative error for analysis. Average organ doses were determined with a weighted average of the recorded organ components, where weighting utilized the ratio of the volume contribution of a region to the total organ volume. Specific organ groups, such as the skeletal system and the lymphatic nodes, were calculated as the average contribution of each component for a single total group value. Organ system doses were calculated as the sum of their organ components, and the total body dose was then calculated

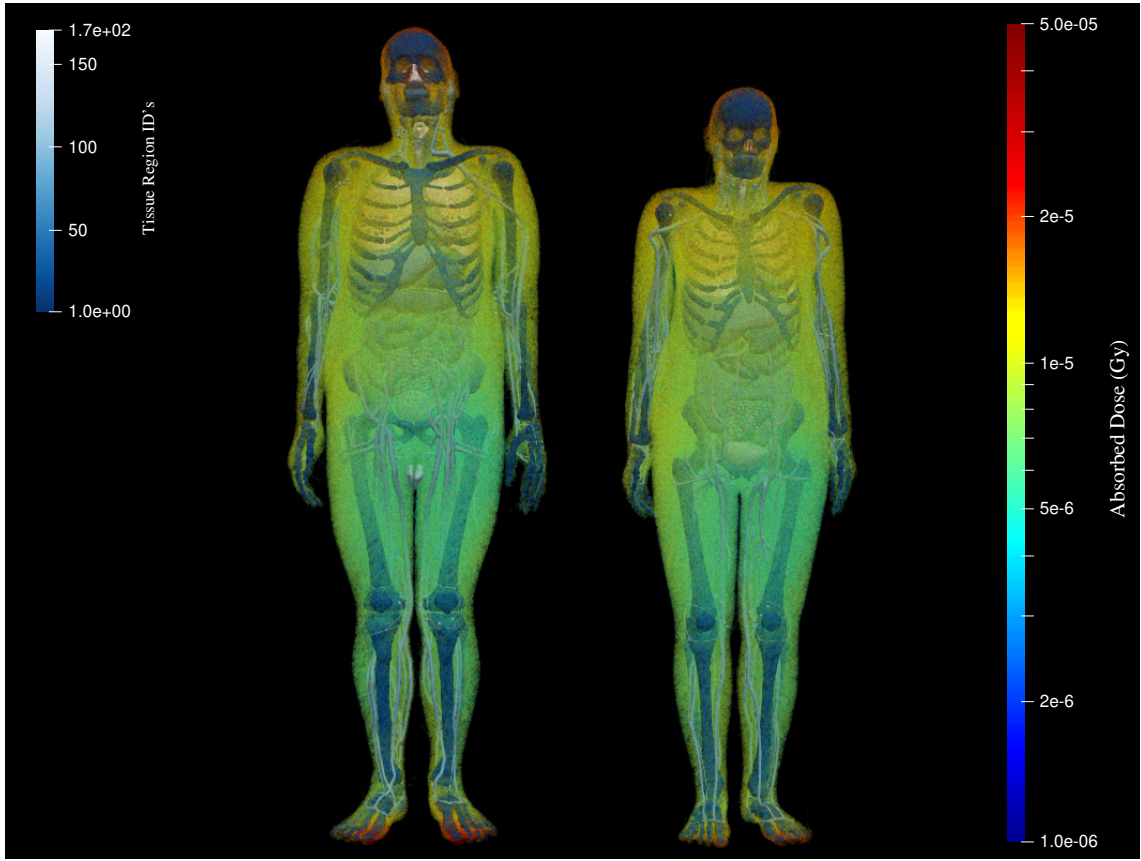


Figure III: Male and female phantoms. The 90th percentile mass and height male (left) and female (right) phantoms were exposed to a simulated IVA spectrum representing space radiation dosage of roughly one full day of exposure in space. Phantoms are shown without skin, muscle, and soft tissue to show internal organs and skeletal frame. The three-dimensional dose distribution of a fraction of the overall dose is overlaid on the phantoms to show the anatomical relation of the dose distribution. All region doses in both phantoms are on the order of μGy .

as the sum of the organ system and extraneous organs not previously included in a system. The average energy deposited for these same categories was determined by using the mass of each region.

Finally, daily dose exposures were used to calculate predictive doses for a 6-9 month and a 3-year mission for male and female crewmembers. A 6-9 month time period would be typical for exposure times during current missions on the ISS while a 3-year mission is the anticipated time frame for an interplanetary exploration mission to Mars. For a 3-year mission to Mars, the dose can be approximately determined by assuming an average Earth to Mars transit time of 200 days, 500 days of exploration on the Mars surface, and 200 days for the return to Earth [29]. GCR fluence is known to be 2-3 times greater outside of LEO, so a factor of 2.5 was used to increase the particle fluence. Prior literature by Zeitlin et. al. describes the interplanetary radiation spectrum as roughly equivalent to that of LEO; as such, calculations utilized dose rates as described by Zeitlin et al. using the fluences described above [30]. The dose incurred from a Mars expedition was then calculated as the sum of the absorbed dose from each stage of the mission. Calculated doses are based on

ISS reference IVA radiation in LEO and thus are not fully reflective of a potential interplanetary exposure; despite this limitation, cumulative doses were calculated and are presented below for further discussion.

Results

The reference computational phantoms were organized into 170 individual regions. Regions ranged from individual organs or structures (e.g. brain, spinal cord, thyroid) to specified sections of an organ or structure (e.g. glandular and adipose breast tissue, spongiosa in the proximal femur). For each of these individual regions, the average absorbed dose and energy deposited are presented in Tables I and II for male and female phantoms, respectively.

The single day whole body absorbed dose for the male and female computational phantoms were determined to be 0.2985 ± 0.0002 mGy/day and 0.3050 ± 0.0002 mGy/day, respectively, as demonstrated in Figure III. Prior studies measuring IVA dose deposition in the ISS Columbus module have reported dose values of 0.286 mGy/day[31]; thus, calculated whole body doses are

within 6.6% of actual measured ISS IVA values. A few systems of interest will be discussed below.

Gastrointestinal System

The complexity of the gastrointestinal system required that 49 individual regions be mapped out for both male and female computational phantoms. For organ totals, the relevant regions were averaged as described above. Regions in the oral cavity were specifically defined including the oral mucosa on the tongue and cheeks. These regions were averaged by their mass component and further averaged with extrathoracic regions representing facial structures for a general oral and facial cavity subset. The colon was further divided into the ascending colon, the right transverse colon, the left transverse colon, the descending colon, the sigmoid colon, and the rectum wall. Those regions were averaged for a total mean colon dose.

The total gastrointestinal system dose was determined as the integral sum of the average doses to the following regions: the oral cavity, esophagus, stomach, small intestines, colon, salivary glands, tonsils, liver, gallbladder, and pancreas. Both male and female phantoms demonstrated highest gastrointestinal organ dose distribution in the salivary glands and the tonsils. For the female computational phantom, the gastrointestinal system received a total dose of 0.2842 ± 0.0004 mGy/day, while the male computational phantom received a total gastrointestinal dose of 0.2705 ± 0.0003 mGy/day.

Circulatory System

The heart wall and blood contents of the heart were delineated into two separate regions. All of the arteries and veins mapped out in the computational phantoms are grouped into a singular artery or vein classification, with no distinction for the different vessels or location in the body. For blood vessel mean doses, arterial and venous doses were averaged together. The total circulatory system mean doses were calculated as the sum of the mass average of the heart and the average of the major vessels.

For the female computational phantom exposure, the heart received an average dose of 0.3017 ± 0.0009 mGy/day, averaged over the heart wall and the heart contents. The arteries and veins received an average dose of 0.3167 ± 0.0006 mGy/day. For the male computational phantom exposure, the heart received an average dose of 0.2987 ± 0.0009 mGy/day, averaged over the heart wall and the heart contents. The arteries and veins received an average dose of 0.3084 ± 0.0005 mGy/day. In total, the female phantom circulatory system received a dose of 0.3107 ± 0.0005 mGy/day, and the male phantom circulatory system received a dose of 0.3041 ± 0.0004 mGy/day.

Brain

For the female computational phantom, the average dose to the brain (excluding eyes, pituitary gland, and spinal cord) was 0.2899 ± 0.0009 mGy/day; for the male computational phantom, the average dose was 0.259 ± 0.001 mGy/day. The brain was not further delineated into individual components; thus, average doses to particular intracranial subregions (for example, individual lobes) is unknown.

Cumulative Dose Predictions for Long-Duration Spaceflight

In a 6-9 month exposure for a female astronaut, predicted cumulative doses were calculated to be 51.2 – 76.8 mGy for the gastrointestinal system, 55.9 – 83.9 mGy for the circulatory system, and 51.9 – 77.9 mGy to the brain. For a male astronaut, the predicted total doses for the same organ sites are 48.7 – 73.0 mGy, 54.7 – 82.1 mGy, and 46.5 – 69.9 mGy, respectively. For whole body exposure, the predicted dose for both female and male astronauts is 54.9 – 82.4 mGy and 53.7 – 80.1 mGy, respectively.

For an exploration mission to Mars, with reference parameters as described above including 400 days in transit and 500 days of surface exploration, the predicted whole body doses were found to be 503.3 mGy and 492.5 mGy for the female and male astronauts, respectively. For the female astronaut, detailed cumulative organ specific doses included 469.0 mGy predicted dose to the gastrointestinal system, 512.6 mGy to the circulatory system, and 476.2 mGy to the brain. For the male astronaut, the predicted cumulative doses for the same organ systems were 446.3 mGy, 501.8 mGy, and 426.7 mGy, respectively.

Discussion

Whole-body daily absorbed dose as calculated by the computational phantom approach was 6.7% of actual recorded ISS values [27, 31, 32]. The remaining error in calculated values is most likely attributed to the spectrum input; here, calculations used measured particle flux and energy averaged over several days. This calculation may be improved in future iterations by refinement of computational inputs and variability derived from considerations such as the solar cycle, shielding, mission parameters and trajectory, and other factors that may alter particle fluence and intravehicular environmental complexity. Even so, these calculations demonstrate a high degree of accuracy particularly when compared to previous approaches. Kuznetsov et. al. compared predicted to measured absorbed dose using a numerical model, SNIP-2016, to calculate the energy spectra of GCR heavy charged particles [33]. They showed a 30% deviation between calculated and measured absorbed dose values from dosimeters [34]. Our results are a significant improvement on previous results.

This work demonstrates the feasibility of performing accurate 3D Monte Carlo simulations to predict the dose topology following an exposure to complex space radiation fields on high-fidelity anatomical male and female computational phantoms. Using novel, high-fidelity phantoms with internal physiology accurate to the scale of a micron in conjunction with the moderator block method [12], this approach demonstrates use of computer-based and beamline-based space radiation calculations to predict on-orbit exposures with a high degree of accuracy. Our approach can thus be introduced into existing Monte Carlo codes and applied to various spaceflight mission scenarios.

While advanced surface phantoms have been used in clinical scenarios, their prior use has been limited in space radiation applications. Surface phantoms can be generated with relative ease from medical imaging (for example, computed tomography (CT) imaging), providing high resolution sources for phantom production and dosimetric calculations. As computational capacity expands in speed and accessibility, high-precision simulations utilizing mesh-phantoms can be performed to provide accurate assessments for highly specific radiation scenarios. The results of this work show the utility of using high performance computers and sophisticated computational models for assessing spaceflight-relevant scenarios. Areas of particular interest for radiobiology and effective dose calculations can be modeled, and dose deposition and track structure analysis on the order of microns and smaller can be simulated and investigated. Mesh computational phantoms have little limit on their resolution capacity, providing the groundwork for computational simulations investigating biological effects on increasingly smaller scales. Areas of interest for adverse radiation effects, such as mucosal linings, lymph nodes, glands, etc., can be modeled in this manner and provide accurate calculations specific to body tissue or organ system.

As mentioned above, surface-type and tetrahedral-type phantoms can be generated from CT or other medical imaging data. As the complexity of structures and layer resolution exceeds imaging capacity, additional modeling input for the phantom would be needed; even so, whole organ systems and well-characterized subregions of organs can be segmented and transformed into a tetrahedral-type phantom. Medical imagery inputs into phantom design and dose-exposure calculations could improve upon personalization of risk assessments for future spaceflight. In essence, this overall capability could enable assessment of individualized exposures that would be incurred by astronaut crews during spaceflight and facilitate the application of a personalized risk assessment in order to better predict and communicate the short- and long-term health outcomes of space radiation exposures.

Conclusions

This novel approach utilizing high-fidelity anatomical computational phantoms in conjunction with the unique

moderator block beamline radiation calculation provides a method of predicting daily and cumulative space radiation dose-exposures to individual organs and whole body exposures with a remarkable degree of accuracy. Tailoring of this method to further improve upon accuracy offers the opportunity for rapid advancement in predictive capability of radiation exposure risks. This could potentially allow for vastly improved understanding of cumulative dose expectations, specific organ exposures and sequelae, and, ultimately, prediction of the impacts and risks associated with space radiation exposure specific to individual crewmembers and design reference missions. As human spaceflight expands outside of LEO, such predictive capability may revolutionize the understanding of health and performance risks and allow for advancement of preventive capabilities to limit health impacts from cumulative space radiation exposure.

Author contributions statement

J.C.C. and M.C. conceived, conducted, and analyzed the experiment. R.S.B. and S.A.C. contributed to the medical discussion and interpretations. All authors contributed to the development and review of the manuscript.

I. ADDITIONAL INFORMATION

J. C. C. and M. C have filed a U.S. Provisional Patent, No. 63/316,832, based on the methods described.

Acknowledgements

Parts of this work were supported by the National Aeronautics and Space Administration through grants 80NSSC21K0544 and 80NSSC21K0273, and LaSPACE through grant number 80NSSC20M0110. The authors would like to thank the Center for Computation & Technology (CCT) at Louisiana State University and the Texas Advanced Computing Center (TACC) at The University of Texas at Austin for providing high performance computing resources that have contributed to the research results reported within this paper. Additionally, the authors would like to thank Hanyang University Radiation Engineering Laboratory (HUREL) at Hanyang University in Seoul, Korea whose phantoms were used in this work.

Data Availability

The datasets generated and analyzed are available from the corresponding author upon reasonable request.

[1] Jeffery C Chancellor, Graham BI Scott, and Jeffrey P Sutton. Space radiation: the number one risk to astronaut health beyond low earth orbit. *Life*, 4(3):491–510, 2014.

[2] Jeffery C Chancellor, Rebecca S Blue, Keith A Cengel, Serena M Auñón-Chancellor, Kathleen H Rubins, Helmut G Katzgraber, and Ann R Kennedy. Limitations in predicting the space radiation health risk for exploration astronauts. *npj Microgravity*, 4(1):1–11, 2018.

[3] Jeffery Chancellor, Craig Nowadly, Jacqueline Williams, Serena Aunon-Chancellor, Megan Chesal, Jayme Looper, and Wayne Newhauser. Everything you wanted to know about space radiation but were afraid to ask. *Journal of Environmental Science and Health, Part C*, 39(2):113–128, 2021. PMID: 33902392.

[4] Ann R Kennedy. Biological effects of space radiation and development of effective countermeasures. *Life sciences in space research*, 1:10–43, 2014.

[5] Jacqueline P Williams, Stephen L Brown, George E Georges, Martin Hauer-Jensen, Richard P Hill, Amy K Huser, David G Kirsch, Thomas J MacVittie, Kathy A Mason, Meetha M Medhora, et al. Animal models for medical countermeasures to radiation exposure. *Radiation research*, 173(4):557–578, 2010.

[6] Gregory A Nelson. Space radiation and human exposures, a primer. *Radiation research*, 185(4):349–358, 2016.

[7] Daniel G Hackam and Donald A Redelmeier. Translation of research evidence from animals to humans. *Jama*, 296(14):1727–1732, 2006.

[8] Pablo Perel, Ian Roberts, Emily Sena, Philipa Wheble, Catherine Briscoe, Peter Sandercock, Malcolm Macleod, Luciano E Mignini, Pradeep Jayaram, and Khalid S Khan. Comparison of treatment effects between animal experiments and clinical trials: systematic review. *Bmj*, 334(7586):197, 2007.

[9] Guenther Reitz, Thomas Berger, Paweł Bilski, R Facius, Michael Hajek, Vladislav Petrov, Monika Puchalska, Dazhuang Zhou, Johannes Bossler, Yury Akatov, Shurshakov Vyacheslav, Paweł Olko, Marta Ptaszkiewicz, Robert Bergmann, Manfred Fugger, Norbert Vana, Rudolf Beujean, Soenke Burmeister, David Bartlett, Luke Hager, Jozsef Palfalvi, Julianna Szabo, Denis O’Sullivan, Hishashi Kitamura, Yukio Uchihori, Nakahiro Yasuda, Aiko Nagamatsu, Hiroko Tawara, Eric Benton, Ramona Gaza, Stephen McKeever, Gabriel Sawakuchi, Eduardo Yukihara, Francis Cucinotta, Edward Semones, Neal Zapp, Jack Miller, and Jan Dettman. Astronaut’s Organ Doses Inferred from Measurements in a Human Phantom Outside the International Space Station. *Radiation Research*, 171:225–235, 2009.

[10] GD Badhwar, W Atwell, FF Badavi, TC Yang, and TF Cleghorn. Space Radiation Absorbed Dose Distribution in a Human Phantom. *Radiation Research*, 157:76–92, 2002.

[11] H Yasuda. Effective Dose Measured with a Life Size Human Phantom in a Low Earth Orbit Mission. *J. Radiat. Res.*, 50:89–96, 2009.

[12] Jeffery C Chancellor, Stephen B Guetersloh, Rebecca S Blue, Keith A Cengel, John R Ford, and Helmut G Katzgraber. Targeted nuclear spallation from moderator block design for a ground-based space radiation analog. *arXiv preprint arXiv:1706.02727*, 2017.

[13] JA Simpson. Elemental and isotopic composition of the galactic cosmic rays. *Annual Review of Nuclear and Particle Science*, 33(1):323–382, 1983.

[14] Steven A Walker, Lawrence W Townsend, and John W Norbury. Heavy ion contributions to organ dose equivalent for the 1977 galactic cosmic ray spectrum. *Advances in Space Research*, 51(9):1792–1799, 2013.

[15] Francis A Cucinotta, Myung-Hee Y Kim, and Lei Ren. Evaluating shielding effectiveness for reducing space radiation cancer risks. *Radiation Measurements*, 41(9–10):1173–1185, 2006.

[16] Choonsik Lee, Daniel Lodwick, Deanna Hasenauer, Jonathan L Williams, Choonik Lee, and Wesley E Bolch. Hybrid computational phantoms of the male and female newborn patient: Nurbs-based whole-body models. *Physics in Medicine & Biology*, 52(12):3309, 2007.

[17] Choonsik Lee, Choonik Lee, Daniel Lodwick, and Wesley E Bolch. Nurbs-based 3-d anthropomorphic computational phantoms for radiation dosimetry applications. *Radiation protection dosimetry*, 127(1–4):227–232, 2007.

[18] Yong Hum Na, Binquan Zhang, Juying Zhang, Peter F Caracappa, and X George Xu. Deformable adult human phantoms for radiation protection dosimetry: anthropometric data representing size distributions of adult worker populations and software algorithms. *Physics in Medicine & Biology*, 55(13):3789, 2010.

[19] CH Kim, YS Yeom, N Petoussi-Henss, M Zankl, WE Bolch, C Lee, C Choi, TT Nguyen, K Eckerman, HS Kim, et al. Icrp publication 145: Adult mesh-type reference computational phantoms. *Annals of the ICRP*, 49(3):13–201, 2020.

[20] Hanjin Lee, Yeon Soo Yeom, Thang Tat Nguyen, Chansoo Choi, Haegin Han, Bangho Shin, Xujia Zhang, Chan Hyeong Kim, Beom Sun Chung, and Maria Zankl. Percentile-specific computational phantoms constructed from icrp mesh-type reference computational phantoms (mrcps). *Physics in Medicine & Biology*, 64(4):045005, 2019.

[21] Chan Hyeong Kim, Jong Hwi Jeong, Wesley E Bolch, Kun-Woo Cho, and Sung Bae Hwang. A polygon-surface reference korean male phantom (psrk-man) and its direct implementation in geant4 monte carlo simulation. *Physics in Medicine & Biology*, 56(10):3137, 2011.

[22] Yeon Soo Yeom, Jong Hwi Jeong, Min Cheol Han, and Chan Hyeong Kim. Tetrahedral-mesh-based computational human phantom for fast monte carlo dose calculations. *Physics in Medicine & Biology*, 59(12):3173, 2014.

[23] Hang Si and A TetGen. A quality tetrahedral mesh generator and a 3d delaunay triangulator. *Cited on*, 61, 2009.

[24] Tatsuhiko Sato, Yosuke Iwamoto, Shintaro Hashimoto, Tatsuhiko Ogawa, Takuya Furuta, Shin-ichiro Abe, Takeshi Kai, Pi-En Tsai, Norihiro Matsuda, Hiroshi Iwase, et al. Features of particle and heavy ion transport code system (phits) version 3.02. *Journal of Nuclear Science and Technology*, 55(6):684–690, 2018.

[25] Alain Boudard, Joseph Cugnon, J-C David, Sylvie Leray, and Davide Mancusi. New potentialities of the liège intranuclear cascade model for reactions induced by nucleons and light charged particles. *Physical Review C*, 87(1):014606, 2013.

[26] Hideo Hirayama, Yoshihito Namito, Walter R Nelson, Alex F Bielajew, Scott J Wilderman, and U Michigan. The egs5 code system. Technical report, United States. Department of Energy, 2005.

[27] Martin Kroupa, Amir Bahadori, Thomas Campbell-Ricketts, Anton Empl, Son Minh Hoang, John Idarraga-Munoz, Ryan Rios, Edward Semones, Nicholas Stoffle, Lukas Tlustos, et al. A semiconductor radiation imaging pixel detector for space radiation dosimetry. *Life sciences in space research*, 6:69–78, 2015.

[28] ICRP. Recommendations of the international commission on radiological protection. *Ann ICRP*, 21, 1990.

[29] Bret G Drake, Stephen J Hoffman, and David W Beaty. Human exploration of mars, design reference architecture 5.0. In *2010 IEEE Aerospace Conference*, pages 1–24. IEEE, 2010.

[30] Cary Zeitlin, Livio Narici, Ryan R Rios, A Rizzo, N Stoffle, DM Hassler, B Ehresmann, RF Wimmer-Schweingruber, J Guo, NA Schwadron, et al. Comparisons of high-linear energy transfer spectra on the iss and in deep space. *Space Weather*, 17(3):396–418, 2019.

[31] Thomas Berger, Sönke Burmeister, Daniel Matthiä, Bartos Przybyla, Günther Reitz, Paweł Bilski, Michael Hajek, Lembit Sihver, Julianna Szabo, Iva Ambrozova, et al. Dosis & dosis 3d: radiation measurements with the dositel instruments onboard the columbus laboratory of the iss in the years 2009–2016. *Journal of Space Weather and Space Climate*, 7:A8, 2017.

[32] Thomas Berger, Bartos Przybyla, Daniel Matthiä, Günther Reitz, Sönke Burmeister, Johannes Labrenz, Paweł Bilski, Tomasz Horwacik, Anna Twardak, Michael Hajek, et al. Dosis & dosis 3d: long-term dose monitoring onboard the columbus laboratory of the international space station (iss). *Journal of Space Weather and Space Climate*, 6:A39, 2016.

[33] NV Kuznetsov, H Popova, and MI Panasyuk. Empirical model of long-time variations of galactic cosmic ray particle fluxes. *Journal of Geophysical Research: Space Physics*, 122(2):1463–1472, 2017.

[34] NV Kuznetsov, MI Panasyuk, and MV Podzolko. Comparison of measured and predicted values of absorbed doses from galactic cosmic rays. *Cosmic Research*, 57:44–47, 2019.

Organ System	Male Phantom	
	<i>Absorbed Dose (mGy/day)</i>	<i>Energy Deposited (mJ/day)</i>
Whole Body Dose	0.2985 ± 0.0002	32.42 ± 0.5
<i>Skeletal System</i>	0.2778 ± 0.0002	3.533 ± 0.003
Spine	0.2722 ± 0.0004	0.576 ± 0.001
Humeri	0.281 ± 0.001	0.1945 ± 0.0007
Femur	0.2754 ± 0.0006	0.510 ± 0.001
<i>GI System</i>	0.2705 ± 0.0003	1.867 ± 0.002
Oral Cavity	0.284 ± 0.003	0.0256 ± 0.0003
Esophagus	0.323 ± 0.002	0.0315 ± 0.0002
Stomach	0.270 ± 0.001	0.1567 ± 0.0006
Small Intestine	0.2730 ± 0.0005	0.4328 ± 0.0008
Colon	0.2582 ± 0.0006	0.2676 ± 0.0006
<i>Circulatory System</i>	0.3041 ± 0.0004	0.890 ± 0.001
Heart	0.2978 ± 0.0009	0.349 ± 0.001
Blood Vessels	0.3084 ± 0.0005	0.5407 ± 0.0008
<i>Lymphatic Nodes</i>	0.293 ± 0.001	0.0720 ± 0.0002
<i>Urogenital System</i>	0.2947 ± 0.0008	0.2933 ± 0.0008
Kidney	0.276 ± 0.001	0.1523 ± 0.0006
Uretha	0.298 ± 0.002	0.00646 ± 0.00005
Bladder	0.312 ± 0.002	0.1023 ± 0.0005
Gonads	0.388 ± 0.005	0.0187 ± 0.0002
Prostate/Uterus	0.316 ± 0.004	0.0072 ± 0.0001
<i>Respiratory System</i>	0.3002 ± 0.0008	0.488 ± 0.001
Trachea	0.350 ± 0.005	0.4744 ± 0.0001
Lungs	0.2999 ± 0.0008	0.468 ± 0.001
Bronchi	0.328 ± 0.003	0.00137 ± 0.00002
Breast	0.303 ± 0.003	0.0139 ± 0.0001
Skin	0.3220 ± 0.0004	1.400 ± 0.002
Eyes	0.303 ± 0.006	0.0052 ± 0.0001
Brain	0.259 ± 0.001	0.940 ± 0.002
Pituitary Gland	0.25 ± 0.01	0.00017 ± 0.00009
Spinal Cord	0.292 ± 0.002	0.0142 ± 0.0002
Thymus	0.348 ± 0.004	0.0181 ± 0.0003
Thyroid	0.371 ± 0.005	0.0134 ± 0.0003
Muscle	0.2992 ± 0.0003	11.89 ± 0.06

Table I: **Organ and organs system doses and energy deposition for the male phantom.** Whole organ doses were determined using volume weighted averages of the calculated regions while organ system doses are the sum of the calculated major organs in each system. The humeri, femur, and lung values are the average values of both right and left sides. The blood vessels value is an average of the doses to the veins and the arteries, and the value for the eyes is the average of the left and right eyes. Energy deposited was determined by using the value for absorbed dose and the mass of the individual regions.

Organ System	Female Phantom	
	Absorbed Dose (mGy/day)	Energy Deposited (mJ/day)
Whole Body Dose	0.3050 ± 0.0002	28.7 ± 0.5
<i>Skeletal System</i>	0.2873 ± 0.0003	2.710 ± 0.002
Spine	0.2850 ± 0.0005	0.4785 ± 0.0009
Humeri	0.286 ± 0.001	0.1575 ± 0.0007
Femur	0.2598 ± 0.007	0.3288 ± 0.0008
<i>GI System</i>	0.2842 ± 0.0004	1.7 ± 0.4
Oral Cavity	0.337 ± 0.004	0.0246 ± 0.0003
Esophagus	0.322 ± 0.002	0.0273 ± 0.0001
Stomach	0.274 ± 0.001	0.1461 ± 0.0006
Small Intestine	0.2863 ± 0.0006	0.3923 ± 0.0007
Colon	0.2717 ± 0.0006	0.2769 ± 0.0006
<i>Circulatory System</i>	0.3107 ± 0.0005	0.673 ± 0.001
Heart	0.3017 ± 0.0009	0.2638 ± 0.0008
Blood Vessels	0.3167 ± 0.0006	0.4098 ± 0.0007
<i>Lymphatic Nodes</i>	0.301 ± 0.001	0.0591 ± 0.0002
<i>Urogenital System</i>	0.2936 ± 0.0008	0.2809 ± 0.0008
Kidney	0.284 ± 0.001	0.1342 ± 0.0005
Uretha	0.299 ± 0.002	0.00609 ± 0.00004
Bladder	0.302 ± 0.002	0.0961 ± 0.0005
Gonads	0.293 ± 0.004	0.00490 ± 0.00007
Prostate/Uterus	0.309 ± 0.002	0.0335 ± 0.0003
<i>Respiratory System</i>	0.3069 ± 0.0007	0.396 ± 0.001
Trachea	0.345 ± 0.004	0.00375 ± 0.00005
Lungs	0.3063 ± 0.0008	0.385 ± 0.001
Bronchi	0.327 ± 0.005	0.00058 ± 0.00009
Breast	0.2899 ± 0.0009	0.2579 ± 0.0008
Skin	0.3260 ± 0.0004	1.018 ± 0.001
Eyes	0.266 ± 0.006	0.00460 ± 0.0001
Brain	0.289 ± 0.001	0.421 ± 0.002
Pituitary Gland	0.31 ± 0.02	0.00022 ± 0.00001
Spinal Cord	0.315 ± 0.003	0.00775 ± 0.00008
Thymus	0.327 ± 0.004	0.0089 ± 0.0001
Thyroid	0.357 ± 0.005	0.0092 ± 0.0001
Muscle	0.3012 ± 0.0003	7.070 ± 0.007

Table II: **Organ and organs system doses and energy deposition for the female phantom.** Whole organ doses were determined using volume weighted averages of the calculated regions while organ system doses are the sum of the calculated major organs in each system. The humeri, femur, and lung values are the average values of both right and left sides. The blood vessels value is an average of the doses to the veins and the arteries, and the value for the eyes is the average of the left and right eyes. Energy deposited was determined by using the value for absorbed dose and the mass of the individual regions.